



ARTICLE

Preparation and Performance of *n*-Dodecane Microencapsulated Phase Change Cold Storage Materials

Pan Zhang, Lingling Xu*, Xin Shi, Zemeng Guo and Jiajia Cheng

College of Materials Science and Engineering, Nanjing Tech University, Nanjing, 211816, China

*Corresponding Author: Lingling Xu. Email: XLL@njtech.edu.cn

Received: 28 February 2022 Accepted: 13 June 2022

ABSTRACT

Cold chain transportation is currently a hot research topic. Since the traditional refrigeration methods lead to the consumption of large amounts of energy, the search for new energy storage materials is a major trend. In the present contribution, *n*-dodecane/PMMA microencapsulated phase change materials were prepared by suspension polymerization for ice-temperature cold chain transportation and their preparation parameters were explored using the encapsulation ratio as optimization indicator. The results show that the *n*-dodecane-containing microcapsules have a maximum encapsulation ratio of 93.2% when using a core-to-wall ratio of 3:1, 5% of emulsifier, 30% of crosslinker, and 2000 rpm of emulsification speed. The phase transition temperature and enthalpy are -2°C and 195.9 kJ/kg, respectively. The microcapsules prepared with the optimized process parameters have good microscopic morphology, high energy storage efficiency, uniform particle size and good thermal stability, making them ideal materials for cold chain transportation.

KEYWORDS

Phase change microcapsules; *n*-dodecane; suspension polymerization; cold storage

1 Introduction

In recent years, energy consumption at a global scale has skyrocketed. Energy saving strategies and the development of new and clean energy resources have become common themes in many countries around the world [1,2]. The cold chain transport sector accounts for an important proportion of energy consumption, which sharply increases each year [3]. Therefore, the development of new and efficient cold storage materials plays a crucial role in energy saving and emission reduction as well as in sustainable development. Phase change materials (PCMs) provide one possible method to store thermal energy. Different phase change materials may be selected depending on the storage temperature requirements. These materials can store thermal energy through a predictable phase change upon cooling at night when the electricity consumption is low, realizing the “peak-shifting and valley-filling” of the power grid, allowing a significant energy saving [4–8].

As carriers of latent thermal energy, PCMs store and release energy through the transformation between solid and liquid phases, with high energy storage density and stable physical and chemical properties [9–14]. Due to their energy storage properties, PCMs are widely used in various energy storage applications such as buildings [15], air conditioners and refrigerators [16], electronic components [17], industrial waste heat



recovery [18], cold-chain storage and transport [19], heat transfer fluids [20], and solar energy [21]. PCMs can be divided into inorganic, organic and composite according to the chemical properties of the constituents [22–24]. Among these three PCM types, the organic ones are favoured by researchers for their low supercooling, low propensity to phase separation, low corrosiveness, stable physico-chemical properties and good solid-state formability [25,26]. Although the advantages of organic PCMs in cold storage applications are outstanding, there are still problems such as reactions with the surrounding environment during the phase change and facile leakage and phase separation after long-term use, which greatly limit their practical application [27]. The application of a microencapsulation strategy to organic PCMs can effectively solve these problems [28–30].

Microencapsulated phase change materials (MEPCMs) are a class of composite phase change storage materials with a core-shell structure, in which microcapsules made of a structurally stable layer of polymer film completely coat the energy storage PCM. MEPCMs work on the principle that when the ambient temperature is higher than the melting temperature of the phase change material, the PCM inside the capsule will absorb heat and melt while keeping its own temperature essentially constant; similarly, when the ambient temperature is lower than the phase change temperature, the PCM will release heat and crystallise, while keeping its own temperature essentially constant [31–37]. In the phase change process, the PCMs can shrink or expand, but the shape of the microcapsules can remain unchanged. Therefore, MEPCMs are shape-stable materials [38]. Common microencapsulation methods include *in situ* polymerisation, interfacial polymerisation, emulsion polymerisation, suspension polymerisation and complex coalescence [39–41]. The microencapsulation of organic PCMs has been the topic of a number of published investigations. For example, Lv et al. [42] prepared a paraffin MEPCMs by *in situ* polymerisation using a low softening point paraffin (46°C) as the PCM and an acrylic copolymer as the shell. The surface morphology, phase change thermal properties and thermal stability of the microcapsules were characterized. Xu et al. [43] obtained a MEPCM with paraffin wax as the PCM and polymethyl methacrylate (PMMA) or a copolymer as the wall material by emulsion polymerisation. Fang et al. [44] synthesised a silica *n*-tetradecane MEPCM by *in situ* interfacial condensation and determined its thermal properties and thermal stability by differential scanning calorimetry and thermogravimetry. Liu et al. [45] synthesised a MEPCM using decanol as the PCM and titanium dioxide (TiO₂) as the encapsulating material for low temperature energy storage by the sol-gel method. DSC results show that the ideal microcapsules melt at 3.87°C with a phase change enthalpy of 61.12 kJ/kg and solidified at –1.32°C with a latent solid enthalpy of 59.54 kJ/kg. In general, the prepared microcapsules have potential for cold energy storage. Han et al. [46] prepared two microcapsules with *n*-tetradecane as the core material and UF (urea-formaldehyde) and PMMA (polymethyl methacrylate) as the shell material using the perforation-curing incision method. The results showed that the phase change enthalpy of the microcapsules is 194.1 kJ/kg at a core to wall ratio of 5.5:1. These MEPCMs are suitable for textile, construction and cold chain transport applications.

The previous research reports have introduced many MEPCMs, but none of these are suitable for cold chain transportation at –2°C~2°C. In the present study, *n*-dodecane/PMMA microcapsules were prepared by suspension polymerization with *n*-dodecane as the core material and poly (methyl methacrylate) as the wall material. The results of the DSC tests showed that the phase change temperature of the microcapsules is –2°C, the phase change enthalpy is 195.9 kJ/kg and the *n*-dodecane encapsulation efficiency is 93.2%. In addition, in order to improve the microcapsule performance, the preparation process parameters were optimized. The effects of core-wall ratio, cross-linking agent dosage, emulsifier dosage and emulsification speed on the microcapsule performance were studied by DSC, SEM, FTIR and particle size analysis. The microcapsules prepared using the optimized parameters, exhibiting good microscopic surface morphology, high energy storage efficiency and large encapsulation ratio, are ideal materials for cold chain transport refrigerant accumulators.

2 Experimental

2.1 Materials

n-Dodecane (C₁₂H₂₆, CP, 98%), with a phase change temperature of −9°C and a phase change enthalpy of 210 kJ/kg, was purchased from Shanghai Macklin Biochemical Co., China. Methyl methacrylate (MMA, C₅H₈O₂, CP, 99.5%) was purchased from Shanghai Lingfeng Chemical Reagent Co., Ltd., China. The styrene/maleic anhydride copolymer (SMA, CP, 80%) was purchased from Shanghai Leather Chemicals Factory, China. Pentaerythritol triacrylate (PETRA, C₁₄H₁₈O₇, AR, 96%) was purchased from Aladdin Bio-Chem Technology Co., China. Azo diisobutyronitrile (AIBN, C₈H₁₂N₄, CP, 98%) was purchased from Shanghai Test Four Dimensions Chemical Co., China. Sodium hydroxide (NaOH, AR, 96%) was purchased from Xilong Science Co., China. The structural formula of methyl methacrylate is given in Fig. 1. All chemicals used in this study, except methyl methacrylate, were used as received.

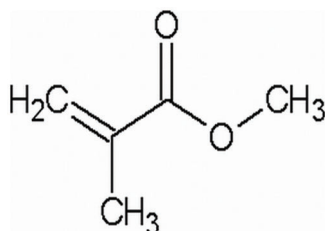


Figure 1: Structural formula of methyl methacrylate (MMA)

2.2 Preparation of MEPCMs

The *n*-dodecane/PMMA MEPCMs were prepared by suspension polymerization [47]. The specific preparation process is described below. The desired amounts (see Table 1) of *n*-dodecane, methyl methacrylate, PETRA and AIBN were mixed in a beaker and ultrasonicated for 10 min to form an oily phase. Meanwhile, distilled water and the SMA emulsifier were weighed and magnetically stirred until forming a homogeneous transparent solution. The oily and aqueous phases were mixed, transferred in a 250 mL three-necked flask and stirred for 15 min at 60°C and 2000 rpm. The mixture was then purged with nitrogen and stirred continuously at a constant speed of 300 rpm for 5 h at 85°C. After the reaction was completed, the product was filtered using a vacuum pump, then the unreacted MMA and the uncoated *n*-dodecane were removed from the product by rinsing 2~3 times with absolute ethanol, then 2 to 3 times with distilled water, and finally dried in an oven at 45°C for 12 h.

Table 1: Preparation ratio of *n*-dodecane/PMMA microcapsules

Sample	Dodecane (g)	MMA (g)	PETRA (g)	SMA (g)	AIBN (g)
M-Dodecane1	10.00	7.00	3.00	1.00	0.30
M-Dodecane2	12.00	5.60	2.40	1.00	0.30
M-Dodecane3	13.33	4.67	2.00	1.00	0.30
M-Dodecane4	14.28	4.00	1.72	1.00	0.30
M-Dodecane5	15.00	3.50	1.50	1.00	0.30
M-PETRA1	15.00	4.50	0.50	1.00	0.30
M-PETRA2	15.00	4.00	1.00	1.00	0.30
M-PETRA3	15.00	3.50	1.50	1.00	0.30

(Continued)

Table 1 (continued)					
Sample	Dodecane (g)	MMA (g)	PETRA (g)	SMA (g)	AIBN (g)
M-PETRA4	15.00	3.00	2.00	1.00	0.30
M-PETRA5	15.00	2.50	2.50	1.00	0.30
SMA1	15.00	3.50	1.50	0.20	0.30
SMA2	15.00	3.50	1.50	0.60	0.30
SMA3	15.00	3.50	1.50	1.00	0.30
SMA4	15.00	3.50	1.50	1.40	0.30
SMA5	15.00	3.50	1.50	1.80	0.30

2.3 Characterization

2.3.1 Differential Scanning Calorimetry (DSC)

The thermal properties of the microcapsules were investigated using a differential scanning calorimeter model DSC 404 F1 Pegasus. The test temperature range was -40°C to 20°C . The samples were subjected to one heating and cooling cycle at $10^{\circ}\text{C}/\text{min}$ in a nitrogen atmosphere. The phase change temperature and latent heat of phase change of the microencapsulated phase material can be obtained from the test results.

2.3.2 Fourier Transform Infrared Spectroscopy (FTIR)

Fourier transform infrared spectra (FTIR) spectra were obtained using a Scientific Nicolet iS5 Fourier transform spectrometer. Powdered specimens of 1~2 mg was ground together with 200 mg of pure KBr, placed in a mold and pressed into transparent sheets on a hydraulic press, and the specimens were tested on an infrared transform spectrometer with a scan number of 32, a resolution of 4 cm^{-1} , and a wavenumber range of $400\sim 4000\text{ cm}^{-1}$.

2.3.3 Microscopic Surface Morphology

The surface morphology of the MEPCMs was analyzed by a JSM-5900 scanning electron microscope (SEM). Before the SEM analysis, a conductive adhesive was applied to the sample holder, the microcapsule powder was evenly adhered to the conductive adhesive, and finally the specimen was sprayed with gold for 2~5 min.

2.3.4 Particle Size Distribution

The MEPCMs were characterized using a Malvern Mastersizer 2000 laser particle size analyzer. The microcapsule powder was diluted with the appropriate amount of distilled water and ultrasonically dispersed before the measurement. The laser particle size analyzer was used in the range of $0.01\sim 3000\text{ }\mu\text{m}$.

2.3.5 TG Analyses

The thermal stability of the microencapsulated PCMs was investigated using a TGA Q500 thermogravimetric analyzer from TA Instruments, USA, with nitrogen atmosphere protection during the test.

2.3.6 Proton Nuclear Magnetic Resonance Spectroscopic Analyses ($^1\text{H-NMR}$)

A Bruker Avance NEO instrument was used for the proton NMR spectroscopic measurements. The polymer was ground into a powder, deuterated chloroform (CDCl_3) was used as the solvent, and the internal standard was tetramethylsilane (TMS), to analyze the chemical shift of the protons in the product.

2.3.7 Encapsulation Ratio

The variation of the MEPCM latent heat as a function of core mass can be described by the covering ratio. The greater the coverage ratio, the better the wall material covers the core material and the higher

the utilisation of the core material. The encapsulation ratio (W) can be calculated using the following formula:

$$W = \frac{\Delta H_{MEPCM}}{\Delta H_{PCM}} \times 100\% \quad (1)$$

where ΔH_{mepcm} is the latent heat value of the microencapsulated PCM (kJ/kg), and ΔH_{pcm} is the latent heat value of the core PCM (*n*-dodecane: 210 kJ/kg).

3 Results and Discussion

3.1 MEPCM Encapsulation Ratio

Fig. 2 shows the encapsulation ratios of microcapsules prepared with different core-to-wall ratios, crosslinker dosages, emulsifier dosages and emulsification speeds.

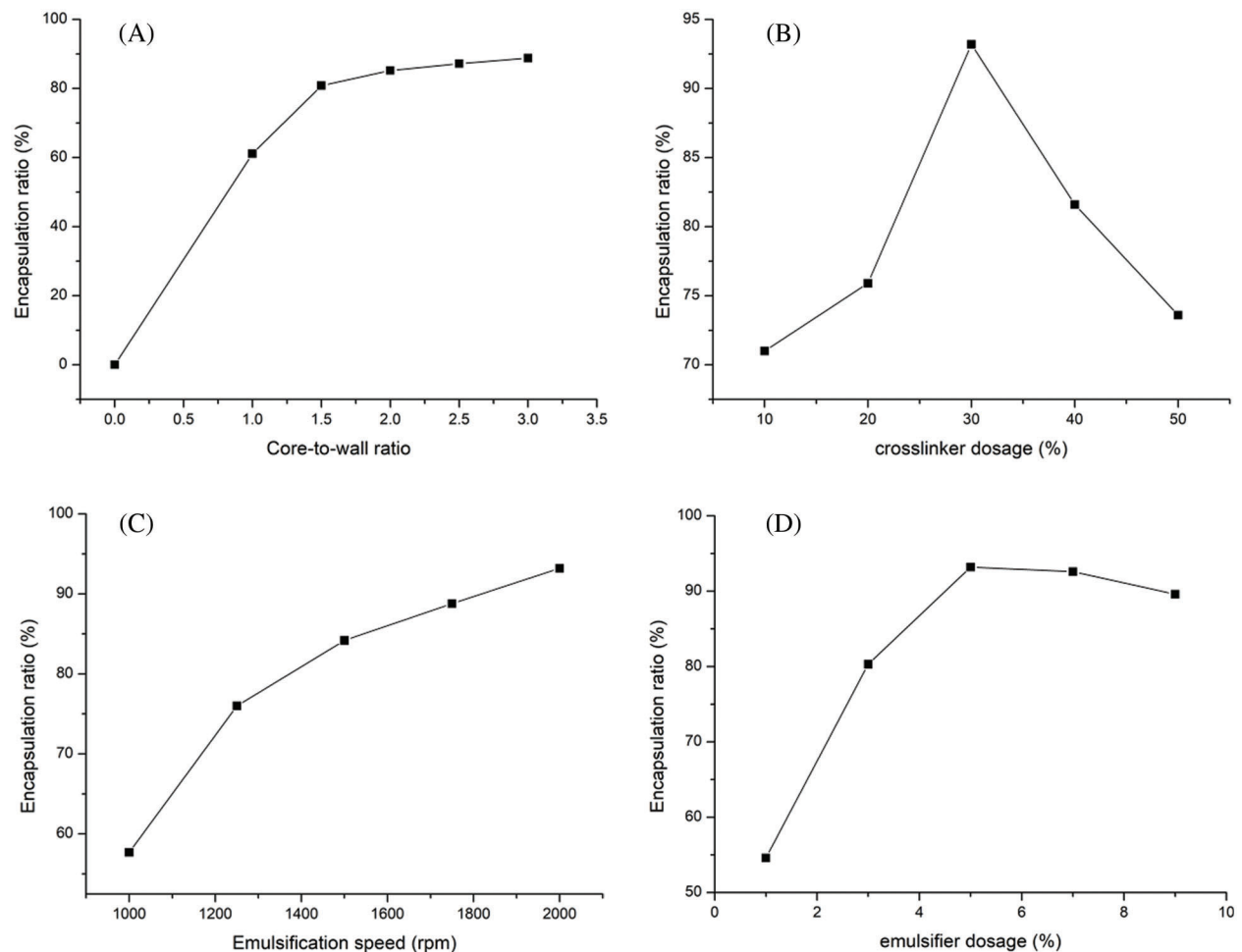


Figure 2: Microcapsules encapsulation ratio of (A) core-to-wall ratio factor, (B) crosslinker dosage factor, (C) emulsification speed factor, (D) emulsifier dosage factor

From Fig. 2A, it can be seen that the encapsulation ratio is proportional to the core-to-wall ratio. When the core-to-wall ratio is 1:1, the encapsulation ratio is 61.1% and the maximum encapsulation ratio is 88.8% for a 3:1 core-to-wall ratio. As shown in Fig. 2B, the smallest encapsulation ratio of 71% corresponds to a

crosslinker dosage of 10% and the largest one of 93.2% corresponds to a crosslinker dosage of 30%. Figs. 2C and 2D show that the encapsulation ratio is largest, reaching 93.2%, when the core-to-wall ratio is 3:1, the crosslinker dosage is 30%, the emulsification speed is 2000 rpm, and the emulsifier dosage is 5%. In order to quantify the effect of each of these four factors on the microencapsulation coverage rate, the variance is listed in Table 2, showing that the effect decreases in the order: Emulsifier dosage > Emulsification speed > Core-to-wall ratio > Crosslinker dosage.

Table 2: Table of encapsulation ratio data and analysis of extreme differences for the four factors

Factor	Encapsulation ratio (%)					Variance (%)
Core-to-wall ratio	61.1	80.8	85.2	87.2	88.8	10.12
Crosslinker dosage	71.0	75.9	93.2	81.6	73.6	7.88
Emulsification speed	57.7	76.0	84.2	88.8	93.2	12.51
Emulsifier dosage	54.6	80.3	93.2	92.6	89.6	32.39

3.2 Effects on the MEPCM Thermal Properties

3.2.1 Effect of Core-to-Wall Ratio on the MEPCM Thermal Properties

In order to investigate the effect of core-to-wall ratio on the MEPCM thermal properties, five sets of experiments were set up for core-to-wall ratios of 1:1, 1.5:1, 2:1, 2.5:1 and 3:1. Fig. 3 shows the DSC curves, and the phase change temperature and latent heat values are listed in Table 3. As can be seen from the data, the phase change enthalpy increased by 32.3% when the core-to-wall ratio was increased from 1:1 to 1.5:1, and by 5.4%, 2.5% and 1.8% when the core-to-wall ratio was further increased to 2:1, 2.5:1 and 3:1, respectively. Obviously, when the core-to-wall ratio is greater than 1:1, the effect of increasing the core-to-wall ratio on the phase change enthalpy of the MEPCM is significantly weaker. This is mainly due to the fact that when the core size increases, the wall material becomes saturated and is no longer sufficient to encapsulate the entire core material, resulting in a less significant increase of the MEPCM phase change enthalpy. Therefore, too large core-to-wall ratios lead to a decrease of the encapsulation ratio, which is not conducive to the preparation of microcapsules.

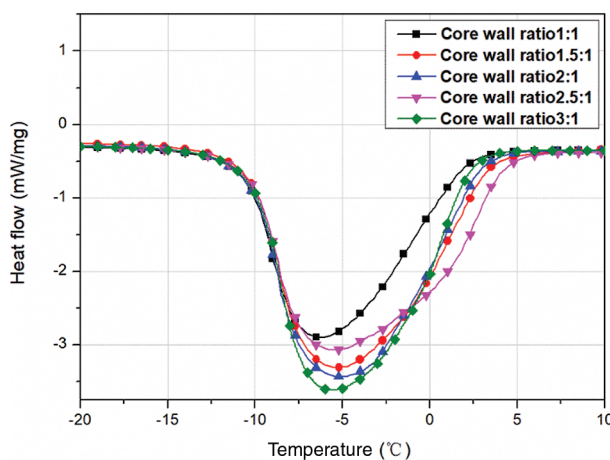


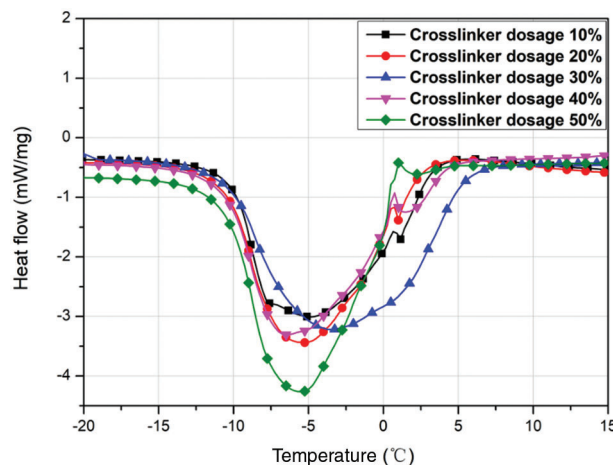
Figure 3: DSC curves of microcapsules prepared with different core-to-wall ratios

Table 3: Thermal property parameters of MEPCMs prepared with different core-to-wall ratios

Core-to-wall ratios	Onset (°C)	Peak (°C)	End (°C)	Latent heat (kJ/kg)
1:1	-10.4	-6.3	2.1	128.3
1.5:1	-10.1	-5.3	3.6	169.7
2:1	-10.2	-5.2	3.2	178.9
2.5:1	-10.1	-5.6	4.2	183.3
3:1	-9.8	-5.8	4.1	186.6

3.2.2 Effect of Crosslinker Dosage on the MEPCM Thermal Properties

The crosslinker dosage is the percentage of the mass of the wall material accounted for by the PETRA crosslinker. Five sets of experiments were set up at crosslinker dosages of 10%, 20%, 30%, 40% and 50%. Fig. 4 shows the corresponding DSC plots, and the data are listed in Table 4. It can be seen that the MEPCM phase change enthalpy is smallest (149.2 kJ/kg) for a crosslinker dosage of 10% and increases when the crosslinker dosage increases to 30%, to reach a maximum value of 195.9 kJ/kg. Further increase of the crosslinker dosage, however, leads to a decrease of the MEPCM phase change enthalpy. This indicates that the optimal crosslinker dosage is 30%. In addition, an important role of the crosslinker is to improve the MEPCM surface morphology. As poly (methyl methacrylate) (PMMA) is a linear polymer, using pure MMA results in a low-density shell material that is prone to leaking. Increasing the cross-linking of the wall material by adding crosslinker not only improves the shell material denseness, but also its strength, which has an important effect on the MEPCM surface morphology.

**Figure 4:** DSC curves of MEPCMs prepared with different crosslinker dosages**Table 4:** Thermal physical parameters of MEPCMs prepared with different crosslinker dosages

Crosslinker dosage (%)	Onset (°C)	Peak (°C)	End (°C)	Latent heat (kJ/kg)
10	-9.9	-4.8	1.6	149.2
20	-10.4	-5.9	1.1	159.5
30	-10.9	-2.0	0.9	195.9
40	-10.8	-6.4	0.6	171.5
50	-10.2	-5.5	0.6	154.6

SEM images of the MEPCM samples with different crosslinker dosages are shown in Fig. 5. When the crosslinker dosage is 0% (Fig. 5a), the outer wall of the MEPCMs was severely broken and depressed. When the crosslinker dosage is 10% (Fig. 5b), the degree of breakage and depression on the MEPCM surface is significantly reduced, but the outer-shell breakage is still serious. Hence, the crosslinker addition improved the MEPCM shell denseness and increased the wall strength, which remains however too low and leads to facile breaking under the action of external forces. In addition, there are more folds and pits on the MEPCM surface. This is due to the fact that the poly (methyl methacrylate) density is greater than that of the methyl methacrylate monomer. Thus, the wall shrinks, and pits appear when MMA is polymerised into PMMA. As the crosslinker dosage was further increased, the MEPCM surface became smoother, with a gradual reduction of the folds and pits. With a crosslinker dosage of 30% (Fig. 5c), the surface of the MEPCMs is almost free of pits, indicating a high degree of cross-linking of the shell material. Continuing to increase the crosslinker dosage, the MEPCM surface morphology (see Figs. 5e and 5f) does not differ much from that of Fig. 5d, but the relative content of the wall material increased due to the excessive crosslinker dosage used, making the MMA polymerisation more efficient and causing the relative content of the wall material to increase and the MEPCM phase change latent heat to decrease, at which point the encapsulation ratio also decreased. Therefore, when the crosslinker dosage is 30%, it is possible to obtain MEPCMs with regular morphology and high strength, which is beneficial to their practical application.

3.2.3 Effect of Emulsifier Dosage on the MEPCM Thermal Properties

Fig. 6 shows the results of DSC analyses of Memos prepared with different emulsifier dosages, and the specific data are shown in Table 5. The emulsifier dosage is the percentage of the total mass of the core and shell material. The results show that the MEPCM phase change enthalpy is 114.6 kJ/kg when the emulsifier dosage is 1% and increased to 169.8 kJ/kg when the dosage was increased to 3%. However, too high dosages lead to a decreasing trend. This is mainly due to an increase of the emulsion system viscosity. The benzene rings on the SMA molecular chain have an obvious blocking effect, which is not conducive to polymer precipitation, resulting in a thin shell material, which is easy to break, resulting in a decrease in phase change enthalpy.

3.3 MEPCM Core-Shell Structure Analysis

Fig. 7 shows the FTIR spectrum of the MEPCM sample prepared with *n*-dodecane, MMA-PETRA and the optimized ratio. Fig. 7a shows the FTIR spectrum of the wall MMA-PETRA polymer. It shows absorption peaks due to the of the $-\text{CH}=\text{CH}_2$ group stretching vibration at 3528 cm^{-1} , to the $-\text{CH}_3$ asymmetric stretching vibration at 2956 cm^{-1} , to the $\text{C}=\text{O}$ stretching vibration at 1733 cm^{-1} , to the carbon-carbon stretching vibration at 1635 cm^{-1} , to the $-\text{CH}_3$ asymmetric deformation at 1443 cm^{-1} and to the $-\text{CH}=\text{CH}_2$ group carbon-hydrogen deformation at 987 and 810 cm^{-1} .

Fig. 7c shows the infrared spectrum of *n*-dodecane, featuring the $-\text{CH}_3$ asymmetric stretching vibration at 2958 cm^{-1} , the $-\text{CH}_2$ asymmetric and symmetric stretching vibrations respectively at 2924 cm^{-1} and 2854 cm^{-1} , the $-\text{CH}_3$ asymmetric deformation at 1463 cm^{-1} and the $-\text{CH}_2$ horizontal rocking vibration at 722 cm^{-1} . All these peaks are consistent with the characteristic peaks of *n*-dodecane [48].

Fig. 7b shows the FTIR spectrum of the *n*-dodecane MEPCM. A comparative analysis of curves (a), (b) and (c) shows that curve (b) contains only the characteristic peaks of both curves (a) and (c) and no other peaks are generated. Fig. 8 shows a SEM image of the optimized MEPCM, featuring a ruptured MEPCM ball. From the combination of the SEM and FTIR analyses, it can be concluded that the polymerised PMMA has successfully encapsulated the *n*-dodecane phase change material to form an MEPCM.

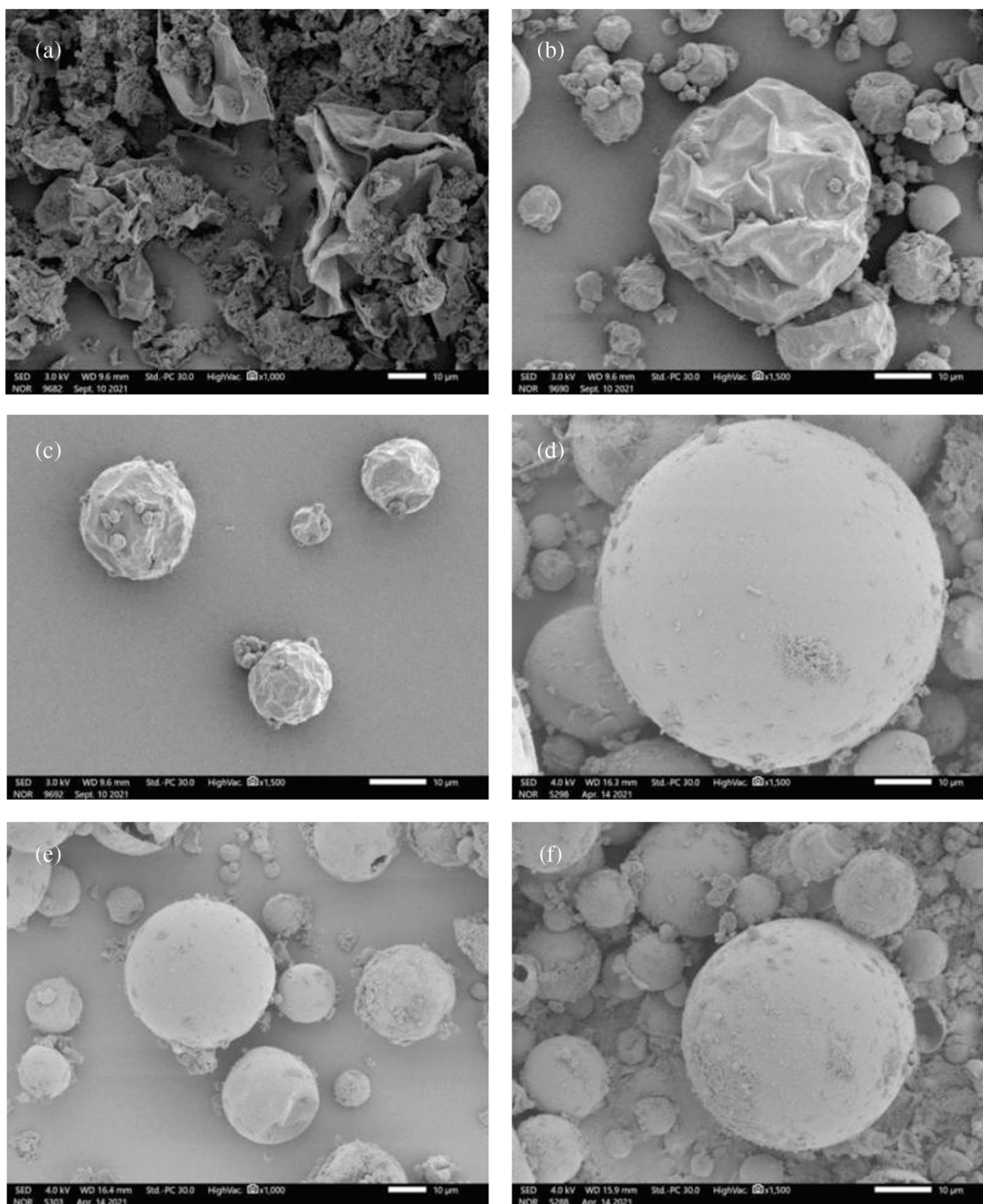


Figure 5: SEM images of MEPCMs with (a) 0%; (b) 10%; (c) 20%; (d) 30%; (e) 40%; (f) 50%

The prepared microcapsules were further analyzed by proton nuclear magnetic resonance spectroscopy. Fig. 9 shows the residual deuterated chloroform resonance at 7.3 ppm and the poly (methyl methacrylate) side chain $-OCH_3$ proton resonance at 3.6 ppm (a). The 1.6 ppm resonance (b) is assigned to the polymer $-CH_3$ side chain protons; the 1.3 ppm resonance (c) is due to the polymer main chain $-CH_2$ protons as well as to *n*-dodecane $-CH_2$ protons. The 0.9 ppm resonance (d) is the characteristic peak of the *n*-dodecane $-CH_3$ protons. Finally, the resonance at 0 ppm is due to the tetramethylsilane (TMS) internal

standard. According to the NMR results, the prepared microcapsules are mainly composed of *n*-dodecane and poly (methyl methacrylate), with the former accounting for the largest proportion (75%).

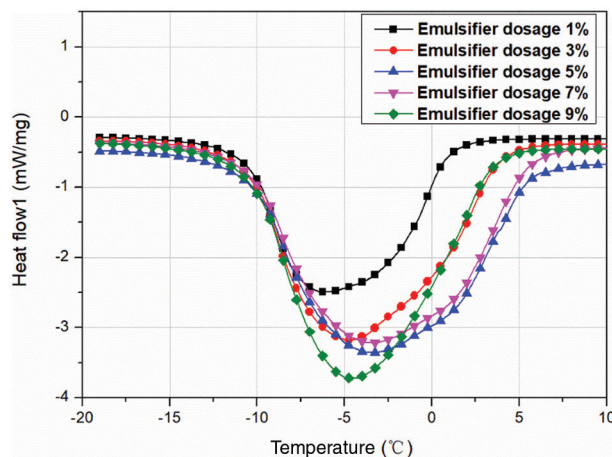


Figure 6: DSC curves of MEPCMs prepared with different emulsifier dosages

Table 5: Thermal physical parameters of MEPCMs prepared with different emulsifier dosages

Emulsifier dosages (%)	Onset (°C)	Peak (°C)	End (°C)	Latent heat (kJ/kg)
1	-10.5	-6.0	1.1	114.6
3	-10.5	-4.8	3.8	168.8
5	-10.9	-2.0	0.9	195.9
7	-10.4	-3.5	5.6	194.6
9	-10.5	-4.6	3.8	188.1

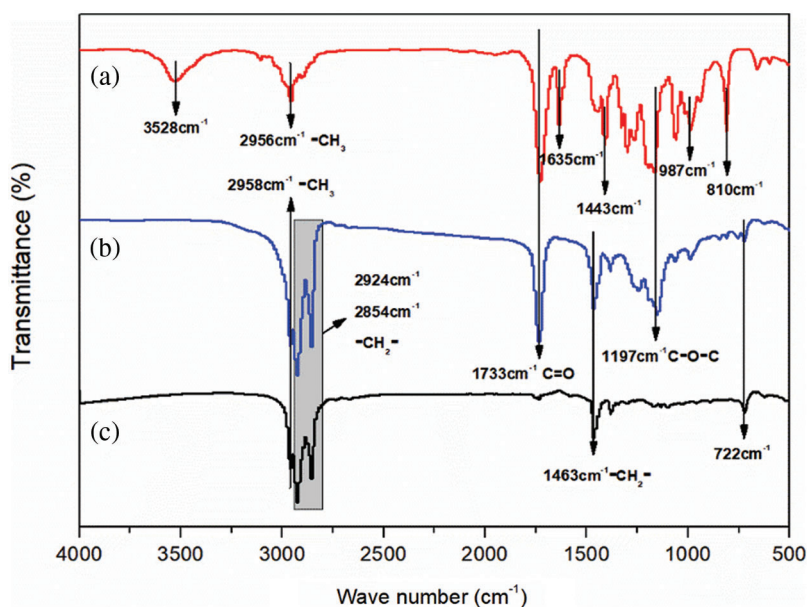


Figure 7: FTIR analysis. (a) MMA-PETRA polymer; (b) microcapsules; (c) *n*-dodecane

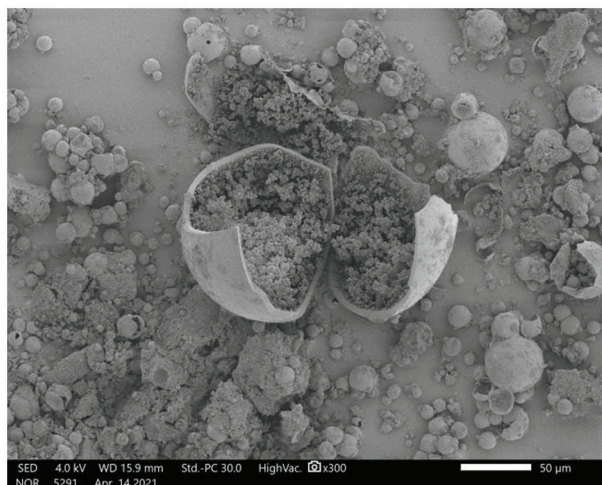


Figure 8: SEM image of the MEPCM prepared with the optimized ratio

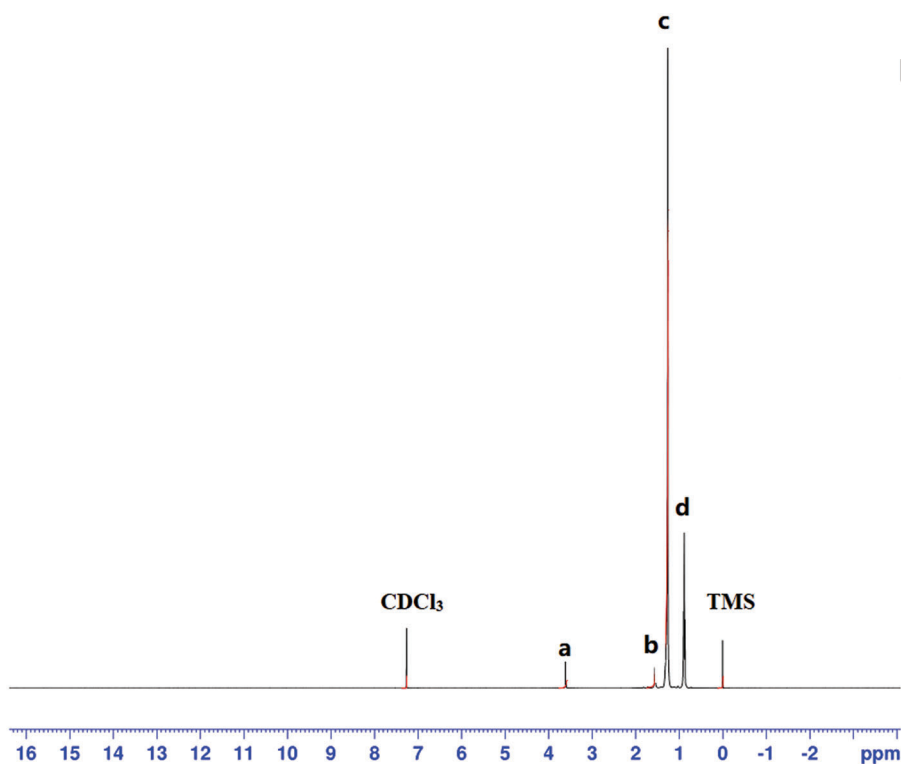


Figure 9: ^1H NMR spectrum of the *n*-dodecane/PMMA MEPCM in CDCl_3

3.4 Effect of the Emulsification Speed on the MEPCM Particle Size

The MEPCM particle size mainly depends on the emulsification speed during emulsification [49]. In order to investigate the effect of this parameter, the MEPCM particle size distribution was analyzed by a laser particle size meter. Fig. 10 shows the particle size distribution of MEPCMs prepared at different emulsification speeds. It can be seen that the distribution shifted to the left and gradually became narrower with an increase of emulsification speed, indicating a gradual decrease of the MEPCM particle

size and an increase of uniformity. Table 6 shows the particle size parameters of MEPCMs prepared at different emulsification speeds. $D(0.5)$ corresponds to the size at which the cumulative percentage of particle size distribution reaches 50%, which is taken as the average particle size of the sample. Span represents the width of the particle size distribution and Uniformity represents the degree of deviation from the middle of the particle size distribution, which are important parameters for characterizing the MEPCM particle size.

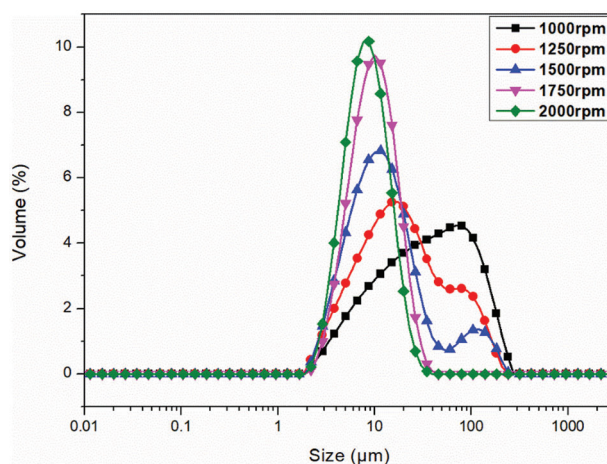


Figure 10: Size distribution curve of microcapsules prepared with different emulsification speeds

Table 6: Size parameters of microcapsules prepared at different emulsification speeds

Emulsification speed (rpm)	$D(0.5)$ (μm)	Span	Uniformity
1000	32.46	4.62	1.43
1250	16.84	4.52	1.30
1500	10.90	3.42	1.06
1750	8.99	1.47	0.46
2000	7.58	1.42	0.44

For emulsification speeds of 1000, 1250, 1500, 1750 and 2000 rpm, $D(0.5)$ is 32.46, 16.84, 10.90, 8.99 and 7.58 μm , respectively. Therefore, the MEPCM particle size decreased with an increase of emulsification speed, being the smallest for an emulsification speed of 2000 rpm. The results also showed that the MEPCM size distribution width tended to decrease with increasing emulsification speed, with Span = 1.42 μm at 2000 rpm, a decrease of 70% compared to the diameter distance of 4.62 μm at 1000 rpm. When the emulsification speed is 2000 rpm, the uniformity is 1.43, which is 69% lower than that of 1000 rpm, indicating that the increase of emulsification speed could not only reduce the MEPCM average particle size, but also improve the uniformity of the particle size distribution, making it more concentrated. In practice, the homogenization rate can be adjusted to obtain MEPCM samples of different particle sizes according to requirements.

3.5 Thermal Stability Analysis

Fig. 11 shows the results of the thermogravimetric analysis (TGA) of the *n*-dodecane/PMMA MEPCM prepared with the optimized process parameters. As can be seen from the figure, the mass loss occurs in two

stages. The first stage occurs in the temperature range 147°C~330°C and leads to a mass loss of 77.88%. The melting point of PMMA is 150°C, and the boiling point of *n*-dodecane is 216°C, therefore the mass loss of this stage is mainly caused by the melting decomposition of the PMMA shell material and by the vaporization of the *n*-dodecane core material. The mass loss rate is highest at 211.07°C, which is near the boiling point of *n*-dodecane, in agreement with vaporization. The decomposition temperature range of the second stage is 390°C~500°C and the mass loss rate is highest at 390.19°C. The mass loss is 21.23% and is attributed to the melting and decomposition of the PMMA combined with crosslinker.

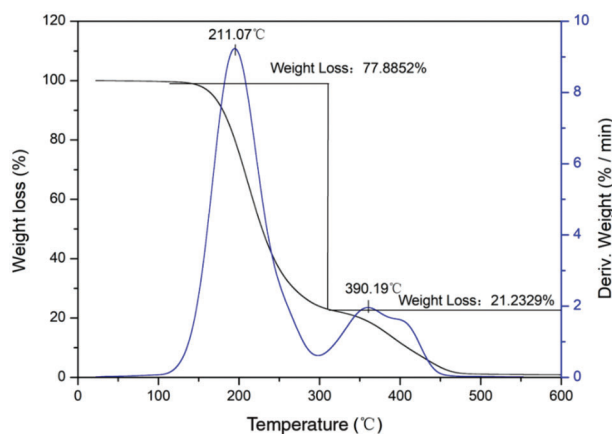


Figure 11: TGA of the microencapsulated phase change material prepared under optimized conditions

The thermal stability analysis shows that the *n*-dodecane/PMMA MEPCM starts to thermally decompose at high temperature in sequence. Firstly, PMMA reached its melting point at 147°C and started to decompose, and as the temperature rose to about 211°C, it reached the boiling point of the core *n*-dodecane material, and *n*-dodecane also decomposed until the temperature reached 390°C, at which point the core *n*-dodecane material decomposition was finished and the mass loss reached 77.8%. Therefore, the temperature in practical application of the *n*-dodecane/PMMA MEPCM should not exceed 150°C.

A certain amount of *n*-dodecane MEPCM powder was subjected to 1, 100 and 200 cold/hot cycles: heating at 50°C for 10 min and then cooling at 0°C for 10 min for each cycle. Fig. 12 shows the DSC curves of the *n*-dodecane MEPCM after three different numbers of cold/hot cycles, and the specific thermal performance parameters are listed in Table 7. When the MEPCM was subjected to one cold and hot cycle, the melting and crystallisation enthalpies were respectively 186.6 and 183.5 kJ/kg. These values decreased after 100 cold/hot cycles to 155.0 and 149.3 kJ/kg, respectively, and then further after 200 cold/hot cycles to 110.3 and 106.4 kJ/kg, respectively. Compared with the material after one cold/hot cycle, the melting and crystallisation enthalpies after 100 cold/hot cycles decreased by 31.6 and 34.2 kJ/kg, corresponding to a 15% decrease of the encapsulation ratio. After 200 cold/hot cycles, the enthalpies decreased by 76.3 and 77.1 kJ/kg, and the encapsulation ratio decreased by 36.3%, while the cladding rate decreased by 36.3%. It can also be seen from the data that the MEPCM subcooling degree remained basically unchanged after 200 cold/hot cycles, indicating that the MEPCM had little effect on the subcooling degree during the 200 cold/hot cycles.

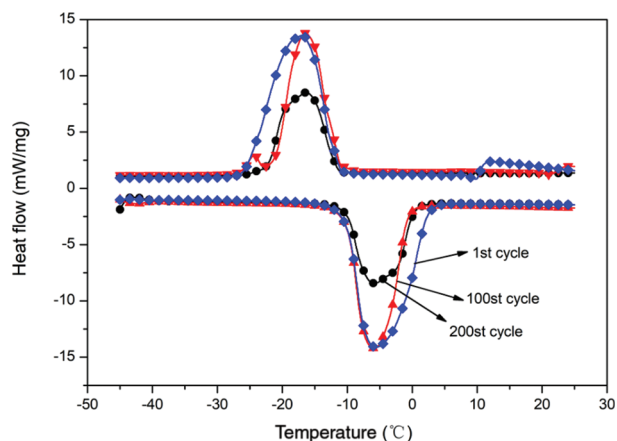


Figure 12: DSC curve of thermal cycle test of microencapsulated phase change material

Table 7: Size parameters of microcapsules prepared at different emulsification speeds

Cycle (times)	T_m (°C)	ΔH_m (kJ/kg)	T_c (°C)	ΔH_c (kJ/kg)	Supercooling (°C)	Encapsulation ratio (%)
1	-5.6	186.6	-15.4	183.5	9.8	88.8
100	-5.8	155.0	-15.5	149.3	9.7	73.8
200	-6.0	110.3	-15.9	106.4	9.9	52.5

4 Conclusions

In this paper, microencapsulated phase change materials were prepared by suspension polymerization using *n*-dodecane as the core phase change material and PMMA as the shell material. The main findings of this work are as follows:

- (1) The results of FITR spectroscopy showed that the prepared MEPCMs contained the characteristic peaks of both the *n*-dodecane core material and the PMMA shell material, and no new peaks were generated, which proved that the polymerized PMMA successfully encapsulated the *n*-dodecane phase change material to form MEPCMs.
- (2) MEPCMs with core-shell structure were successfully prepared with encapsulation ratios up to 93.2%.
- (3) In order to prepare MEPCMs with better performance, the effects of four factors, namely, core-to-wall ratio, crosslinker dosage, emulsification speed, and emulsifier dosage, on the MEPCM performance were analyzed. The DSC results showed that the highest encapsulation ratio (93.2%) was obtained for a core-to-wall ratio of 3:1, a crosslinker dosage of 30% (as a percentage of the mass of the wall material), a homogenization rate of 2000 rpm, and an emulsifier dosage of 5% (as a percentage of the total mass of the wall material and the core material). The phase transition temperature and phase transition enthalpy of the optimized material were -2°C and 195.9 kJ/kg, respectively.
- (4) The SEM results showed that the amount of cross-linking agent had a great influence on the MEPCM surface morphology. When the amount of cross-linking agent was 30%, the MEPCM surface was smooth with good morphology. In addition, the results of particle size analysis showed that the prepared MEPCMs had the smallest average particle size and the narrowest particle size distribution when using a homogenization rate of 2000 rpm.

- (5) The TGA characterization of the MEPCM prepared under the optimized conditions showed that melting and decomposition started at 147°C and *n*-dodecane began to vaporize at about 211°C. Therefore, the application temperature of MEPCMs based on *n*-dodecane/PMMA should not exceed 150°C. In addition, the MEPCM thermal cycling stability was also tested. The results showed that the melting and crystallization enthalpies decreased by 15% after 100 cold/hot cycles, and further by 36.3% after 200 cold/hot cycles.
- (6) The *n*-dodecane/PMMA MEPCM synthesized and under optimized conditions exhibit excellent thermal properties, large phase change enthalpies and good microscopic morphology, which meet the requirements of cold storage and are ideal materials for the cold storage field.

Funding Statement: This work was supported by the National Key Research and Development Program of china (No. 2018YFD1101005) and the Priority Academic Program Development of Jiangsu Higher Education Institutions (PAPD).

Conflicts of Interest: The authors declare that they have no conflicts of interest to report regarding the present study.

References

1. Zhu, Y., Liang, S., Chen, K. (2015). Preparation and properties of nanoencapsulated *n*-octadecane phase change material with organosilica shell for thermal energy storage. *Energy Conversion & Management*, 105, 908–917. DOI 10.1016/j.enconman.2015.08.048.
2. Cunha, J. (2015). Thermal energy storage for low and medium temperature applications using phase change materials—A review. *Applied Energy*, 177, 227–238. DOI 10.1016/j.apenergy.2016.05.097.
3. Huang, Y., Zhang, X., University, S. (2015). Research progress of the application of cold storage technology in food cold chain logistics. *Packaging Engineering*, 36(15), 23–29.
4. Lefebvre, D., Tezel, F. (2017). A review of energy storage technologies with a focus on adsorption thermal energy storage processes for heating applications. *Renewable and Sustainable Energy Reviews*, 67, 116–125. DOI 10.1016/j.rser.2016.08.019.
5. Wang, C., Lin, T., Li, N. (2016). Heat transfer enhancement of phase change composite material: Copper foam/paraffin. *Renewable Energy*, 96, 960–965. DOI 10.1016/j.renene.2016.04.039.
6. Zhao, Y., Zhang, X., Xu, X. (2020). Development of composite phase change cold storage material and its application in vaccine cold storage equipment. *The Journal of Energy Storage*, 30, 101455. DOI 10.1016/j.est.2020.101455.
7. Sari, A., Karaipekli, A., Eroğlu, R. (2013). Erythritol tetra myristate and erythritol tetra laurate as novel phase change materials for Low temperature thermal energy storage. *Energy Sources, Part A: Recovery, Utilization, and Environmental Effects*, 35(14), 1285–1295. DOI 10.1080/15567036.2010.516323.
8. Zhao, L., Yu, Q., Li, M. (2021). Preparation and thermal properties of low-temperature composite phase-change materials based on a binary eutectic mixture with expanded graphite: Effect of particle size and mass fraction. *Journal of Energy Storage*, 40, 102778. DOI 10.1016/j.est.2021.102778.
9. Suresh, C., Saini, R. P. (2020). Thermal performance of sensible and latent heat thermal energy storage systems. *International Journal of Energy Research*, 44(6), 4743–4758. DOI 10.1002/er.5255.
10. Nazir, H., Batool, M., Osorio, F. (2019). Recent developments in phase change materials for energy storage applications. *International Journal of Heat and Mass Transfer*, 129, 491–523. DOI 10.1016/j.ijheatmasstransfer.2018.09.126.
11. Veerakumar, C., Sreekumar, A. (2016). Phase change material based cold thermal energy storage: Materials, techniques and applications. *International Journal of Refrigeration*, 67, 271–289. DOI 10.1016/j.ijrefrig.2015.12.005.
12. Zhang, N., Yuan, Y., Cao, X. (2018). Latent heat thermal energy storage systems with solid–Liquid phase change materials. *Advanced Engineering Materials*, 20(6), 1700753. DOI 10.1002/adem.201700753.

13. Sarbu, I., Dorca, A. (2018). Review on heat transfer analysis in thermal energy storage using latent heat storage systems and phase change materials. *International Journal of Energy Research*, 43(1), 29–64. DOI 10.1002/er.4196.
14. Safari, A., Saidur, R., Sulaiman, F. A. (2017). A review on supercooling of phase change materials in thermal energy storage systems. *Renewable & Sustainable Energy Reviews*, 70, 905–919. DOI 10.1016/j.rser.2016.11.272.
15. Bari, R. D., Horn, R., Nienborg, B. (2020). The environmental potential of phase change materials in building applications. *Energies*, 13, 3045. DOI 10.3390/en13123045.
16. Dong, Y., Liu, Y., Wang, D. (2019). Review of latent thermal energy storage systems for solar air-conditioning systems. *International Journal of Energy Research*, 44(6), 669–707.
17. Kumar, A., Kothari, R., Sahu, S. (2021). Thermal performance of heat sink using nano-enhanced phase change material (NePCM) for cooling of electronic components. *Microelectronics Reliability*, 121, 114144. DOI 10.1016/j.microrel.2021.114144.
18. Li, Z., Lu, Y., Huang, R., Chang, J., Yu, X. et al. (2020). Applications and technological challenges for heat recovery, storage and utilisation with latent thermal energy storage. *Applied Energy*, 20, 116277.
19. Zhao, Y., Zhang, X., Xu, X. (2019). Application and research progress of cold storage technology in cold chain transportation and distribution. *Journal of Thermal Analysis and Calorimetry*, 139(2), 1419–1434. DOI 10.1007/s10973-019-08400-8.
20. Wang, F., Lin, W., Ling, Z., Fang, X. (2019). A comprehensive review on phase change material emulsions: Fabrication, characteristics, and heat transfer performance. *Solar Energy Materials and Solar Cells*, 191, 218–234. DOI 10.1016/j.solmat.2018.11.016.
21. Javadi, F. S., Metselaar, H., Ganesan, P. (2020). Performance improvement of solar thermal systems integrated with phase change materials (PCM). *Solar Energy*, 206, 330–352. DOI 10.1016/j.solener.2020.05.106.
22. Nie, B., Trujillo, A. P., Zou, B., Liu, J., Zhang, T. et al. (2020). Review on phase change materials for cold thermal energy storage applications. *Renewable and Sustainable Energy Reviews*, 134, 110340. DOI 10.1016/j.rser.2020.110340.
23. Zhang, X. Q. (2019). Research progress and applications of phase change materials for energy storage. *Modern Chemical Industry*, 39(4), 67–70.
24. Umair, M. M., Zhang, Y., Iqbal, K., Zhang, S., Tang, B. et al. (2018). Novel strategies and supporting materials applied to shape-stabilize organic phase change materials for thermal energy storage. *Applied Energy*, 235, 846–873. DOI 10.1016/j.apenergy.2018.11.017.
25. Aslfattahi, N., Saidur, R., Arifuzzaman, A., Bimbo, N., Bouscarrat, L. et al. (2018). Experimental investigation of energy storage properties and thermal conductivity of a novel organic phase change material/MXene as a new class of nanocomposites. *Journal of Energy Storage*, 27, 101111–101115.
26. Yang, T. R., Sun, Q., Wennersten, R., Lin, C. (2018). Review of phase change materials for cold thermal energy storage. *Journal of Engineering Thermophysics*, 39(3), 567–573.
27. Alva, G., Lin, S. (2017). Characterization and applications of microencapsulated phase change materials in thermal energy storage. *Energy and Buildings*, 144, 276–294. DOI 10.1016/j.enbuild.2017.03.063.
28. Darkwa, J. K. (2018). Review of solid-liquid phase change materials and their encapsulation technologies. *Renewable & Sustainable Energy Reviews*, 48, 373–391. DOI 10.1016/j.rser.2015.04.044.
29. Salunkhe, P. B., Shembekar, P. S. (2012). A review on effect of phase change material encapsulation on the thermal performance of a system. *Renewable and Sustainable Energy Reviews*, 16(8), 5603–5616. DOI 10.1016/j.rser.2012.05.037.
30. Wang, G., Liu, Z., Jiang, T. (2021). Impact evaluation of cold heat transfer fluid temperature on heat storage and mechanical behaviours of an energy storage system using phase-change material. *International Journal of Thermophysics*, 42(5), 1–18. DOI 10.1007/s10765-021-02823-y.
31. Gang, L., Hwang, Y., Radermacher, R. (2012). Review of cold storage materials for air conditioning application. *International Journal of Refrigeration*, 35(8), 2053–2077. DOI 10.1016/j.ijrefrig.2012.06.003.
32. Giro-Paloma, J., Martínez, M., Cabeza, L. F. (2016). Types, methods, techniques, and applications for microencapsulated phase change materials (MPCM). *Renewable and Sustainable Energy Reviews*, 53, 1059–1075. DOI 10.1016/j.rser.2015.09.040.

33. Aj, A., Sms, A., Mf, B. (2014). A review of microencapsulation methods of phase change materials (PCMs) as a thermal energy storage (TES) medium. *Renewable and Sustainable Energy Reviews*, 31, 531–542. DOI 10.1016/j.rser.2013.12.033.
34. Alva, G., Lin, Y., Liu, L. (2014). Morphological characterization and applications of phase change materials in thermal energy storage. *Energy & Buildings*, 72, 128–145.
35. Cao, V. D., Pilehvar, S., Salas-Bringas, C. (2014). Microencapsulated phase change materials for enhancing the thermal performance of portland cement concrete and geopolymer concrete for passive building applications. *Energy Conversion & Management*, 133, 56–66. DOI 10.1016/j.enconman.2016.11.061.
36. Ren, M., Wen, X., Gao, X. (2021). Thermal and mechanical properties of ultra-high performance concrete incorporated with microencapsulated phase change material. *Construction and Building Materials*, 273(1), 121714. DOI 10.1016/j.conbuildmat.2020.121714.
37. Wu, N., Xu, L., Zhang, C. (2018). The influence of emulsifiers on preparation and properties of microencapsules of melamine-urea-formaldehyde resins with n-odecanol as phase change material. *Advances in Polymer Technology*, 37(8), 3492–3498. DOI 10.1002/adv.22133.
38. Delgado, M., Lázaro, A., Mazo, J. (2012). Review on phase change material emulsions and microencapsulated phase change material slurries: Materials, heat transfer studies and applications. *Renewable and Sustainable Energy Reviews*, 16(1), 253–273. DOI 10.1016/j.rser.2011.07.152.
39. Shan, X., Shiwei, L. I., Wang, F., Zhao, W., Yan, J. (2011). Preparation of paraffin microcapsule phase change materials by insitu polymerization. *Electronic Science and Technology*, 24(9), 94–96. DOI 10.16180/j.cnki.issn1007-7820.2011.09.012.
40. He, F., Wang, X., Wu, D. (2014). New approach for sol-gel synthesis of microencapsulated n-octadecane phase change material with silica wall using sodium silicate precursor. *Energy*, 67, 223–233. DOI 10.1016/j.energy.2013.11.088.
41. Liang, C., Xu, L., Shang, H. (2009). Microencapsulation of butyl stearate as a phase change material by interfacial polycondensation in a polyurea system. *Energy Conversion and Management*, 50(3), 723–729. DOI 10.1016/j.enconman.2008.09.044.
42. Lv, X., Guo, P., Liu, H. (2018). Preparation of paraffin-based phase-change microcapsules and application in geopolymer coating. *Journal of Coatings Technology and Research*, 15(4), 867–874. DOI 10.1007/s11998-018-0071-6.
43. Xu, D., Yang, R. (2019). Efficient preparation and characterization of paraffin-based microcapsules by emulsion polymerization. *Journal of Applied Polymer Science*, 136(21), 47552. DOI 10.1002/app.47552.
44. Fang, Y., Wei, H., Liang, X. (2016). Preparation and thermal performance of silica/n-tetradecane microencapsulated phase change material for cold energy storage. *Energy & Fuels*, 30(11), 9652–9657. DOI 10.1021/acs.energyfuels.6b01799.
45. Liu, Y., Chen, Y. (2021). Synthesis and characteristics of microencapsulated decanol with TiO₂ shell as composites for cold energy storage. *Materials Science*, 27(4), 24721. DOI 10.5755/j02.ms.24721.
46. Han, P., Lu, L., Qiu, X. (2015). Preparation and characterization of macrocapsules containing microencapsulated PCMs (phase change materials) for thermal energy storage. *Energy*, 91, 531–539. DOI 10.1016/j.energy.2015.08.001.
47. Qiu, X., Lu, L., Wang, J. (2015). Preparation and characterization of microencapsulated n-octadecane as phase change material with different n-butyl methacrylate-based copolymer shells. *Solar Energy Materials and Solar Cells*, 128, 102–111. DOI 10.1016/j.solmat.2014.05.020.
48. Levitskaia, T. G., Peterson, J. M., Campbell, E. L. (2013). Fourier transform infrared spectroscopy and multivariate analysis for online monitoring of dibutyl phosphate degradation product in tributyl phosphate/n-dodecane/Nitric acid solvent. *Industrial & Engineering Chemistry Research*, 52(49), 17607–17617. DOI 10.1021/ie402722n.
49. Amp, K. Z., Yuan, X. (2012). Preparation and characterization of melamine-formaldehyde resin micro-and nanocapsules filled with n-dodecane. *Journal of Macromolecular Science Part B*, 51(10), 1976–1990. DOI 10.1080/00222348.2012.661663.